Available online at www.sciencedirect.com
SCIENCE DIRECT®
ELSEVIER
Nuclear Instruments and Methods in Physics Research B 227 (2005) 233–250
NIM B
Beam Interactions with Materials & Atoms
www.elsevier.com/locate/nimb

Electron and neutron scattering from polymer films at high momentum transfer

M. Vos [a,*], C.A. Chatzidimitriou-Dreismann [b], T. Abdul-Redah [c,d], J. Mayers [d]

[a] *Atomic and Molecular Physics Laboratories, Research School of Physical Sciences and Engineering, The Australian National University, Canberra ACT 0200, Australia*
[b] *Institute of Chemistry, Stranski-Laboratory, Technical University of Berlin, Strasse des 17. Juni 112, Berlin D-10623, Germany*
[c] *Physics Laboratory, The University of Kent at Canterbury, Canterbury, Kent CT2 7NR, United Kingdom*
[d] *ISIS Facility, Rutherford Appleton Laboratory, Chilton, Didcot OX11 0QX, United Kingdom*

Received 8 March 2004; received in revised form 27 August 2004

Abstract

Neutrons have been used in the past to measure Compton profiles of atomic motion. Recently it was found that similar information can be obtained using electron scattering experiments. In particular formvar and polyethylene were studied using both techniques, thus considerably extending the first results reported recently [C.A. Chatzidimitriou-Dreismann et al., Phys. Rev. Lett. 91 (2003) 57403]. In this paper we review the underlying theoretical framework and compare the experimental realization of both techniques. The various steps required to analyze the data are outlined. Both in the neutron and electron experiments we found anomalous low intensities of the hydrogen contribution to the spectrum.

PACS: 78.70.−g; 61.14.−x; 61.12.−q; 03.65.Ud
Keywords: Electron scattering; Neutron scattering; Momentum distributions; Entanglement

1. Introduction

Scattering experiments are one of the main tools in physics to study the structure of matter. In these experiments an incoming particle interacts with the target and transfers a certain amount of energy $\hbar\omega$ and momentum $\hbar\boldsymbol{q}$ to the target. For condensed matter scattering experiments at small momentum transfer, the intensity originating from different atoms adds coherently and one obtains diffraction. At high momentum transfer ($qa \gg 1$, where a is the interatomic separation) the incoming particle interacts incoherently with the sample and scatters from an individual atom.

* Corresponding author. Tel.: +61 2 61254985; fax: +61 2 61252452.
E-mail address: maarten.vos@anu.edu.au (M. Vos).

0168-583X/$ - see front matter
doi:10.1016/j.nimb.2004.09.003

Electron scattering at high momentum transfer was studied by Boersch et al. [1] as early as 1967. In this work the authors established that the energy loss of fast (20–40 keV) electrons scattered quasi-elastically over large angles was equal to $(\hbar q)^2/2M$ i.e. consistent with the electrons transferring momentum to a single atom (with mass M), rather than the whole crystal. Besides this small energy loss, also a broadening of the energy distribution was observed. Unfortunately it was not realized that this broadening of the quasi-elastic peak could be seen as the Compton profile of the momentum distribution of the scattering atom in its ground state. Especially for carbon the quasi-elastic peak width was much larger than expected from the energy resolution alone. This width was interpreted correctly in terms of Doppler broadening, but instead of comparing it to the quantum-mechanical zero point motion of the nuclei, they assumed simply that each atom had a kinetic energy of $3kT/2$. In this way Boersch et al. derived a sample temperature of up to 1600 K. This surprisingly high temperature was attributed to electron beam heating. Some recent work [2] on quasi-elastic scattering of keV electrons still uses the same arguments as in the original paper by Boersch et al.

In contrast scattering experiments using neutrons were designed to measure the ground state momentum distributions of quantum systems. As early as 1966 Hohenberg and Platzman [3] proposed to study the momentum distributions in superfluid ^{4}He mixtures in scattering experiments using neutrons with energies around 1 eV. For more strongly bound systems, such as crystals, more energetic neutrons (i.e. larger momentum transfer) are required. The first neutron Compton scattering from solids was realized by Rauh and Watanabe [4] in 1984, and this technique has since been used for a series of studies over the last 20 years [5].

First a remark about the nomenclature. Within neutron research the neutron Compton experiments are referred to as deep inelastic scattering. In elastic neutron scattering (e.g. diffraction from a crystal) momentum is transferred to the target as a whole, and hence the energy of the outgoing neutron is the same as that of the incoming neutron. In deep inelastic scattering the incoming neutron interacts with a single atom within the target, and hence transfers both energy and momentum. The energy of the outgoing neutron is thus reduced, hence the name (deep-) inelastic scattering.

In the field of electron scattering this type of experiments are usually called elastic scattering experiments. The scattered electron interacts with only a single nucleus and one can consider the collision in the center-of-mass frame of this electron-nucleus system. In this system the kinetic energy of the electron does not change, hence the scattering is called 'elastic'. Due to the small mass of the electron the difference between the center-of-mass system and laboratory system is small and the energy loss in the laboratory frame is usually negligibly small. Within the field of electron scattering the term 'inelastic scattering' refers to collisions in which the target electronic system is left in an excited state. Thus, in spite of the fact that the nomenclature suggests that the electron and neutron scattering processes are fundamentally different in nature, they are very similar indeed. For clarity we will use the term quasi-elastic scattering for electrons deflected from an ion core with noticeable energy loss.

As the energy transfer depends on the atomic mass one can separate the contribution of neutrons scattered from protons from the contribution of neutrons scattered from heavier elements. For many materials that contain hydrogen (water [6], metal hydrides [7,8], polymers [9], amphiphilic materials [10]) persistent anomalies were found when relating the observed peak areas with predictions based on neutron scattering theory. It was suggested that short-lived quantum entanglement of protons was the cause of these discrepancies [6].

In a transmission electron scattering experiment on formvar (formvar is a trade name for polyvinyl formal, a polymer with monomer unit $C_8O_2H_{14}$) it was shown that electron scattering can measure the Compton profiles of the nuclear motion in a similar way as neutron scattering does [11]. Again the contributions from protons could be separated from that of heavier elements. Surprisingly the electron experiment showed again a deviations of the measured hydrogen intensity from the conven-

tionally expected one. Thus it is unlikely that the anomaly can be explained as an experimental artifact due to the completely different realization of the neutrons and electrons experiment. Also explanations based on specific properties of the scattering process are severely restricted as the nature of projectile-target interaction is completely different (the (long-range) Coulomb interaction for electrons and the (short-range) strong interaction for neutrons). The present combined study by electron scattering and neutron scattering aims to establish more firmly the fact that both techniques measure essentially the same quantity. Here we present data from formvar and polyethylene films studied both by neutron and electron scattering. Some of the experimental results and the implications of the formvar data for proton entanglement were discussed in a separate letter [12].

The anomalous neutron scattering experiments are currently hotly debated, see for example [13–19]. It is not the aim of this paper to explain the anomaly. Rather we want to establish the similarities and differences between the electron and neutron scattering experiments, and establish which parameters, used in models describing these experiments, differ (e.g. scattering time, coherence length). An understanding of the physics of both scattering experiments may help in designing tests that can differentiate between different models. Hence the paper is organized in the following way. We first review the electron and neutron scattering experiments within the same theoretical framework. We then describe the completely different experimental realization of both techniques, discuss the influence of multiple scattering, and present the results for two different polymers: formvar and polyethylene. Finally we investigate the effects of radiation damage for the electron scattering case.

2. Theory

The theoretical foundation of this type of scattering experiments was established by Van Hove [20] for the case of neutron scattering. Here we reproduce this derivation, pointing out the difference and similarities between electron and neutron scattering experiments. If the first Born approximation is valid the double differential scattering cross section can be written as

$$\frac{\mathrm{d}^2\sigma}{\mathrm{d}\Omega\,\mathrm{d}\varepsilon} = \frac{m^2}{4\pi^2\hbar^5}\frac{k_1}{k_0}W(\boldsymbol{q})S(\boldsymbol{q},\omega), \tag{1}$$

in which m is the mass of the scattered particle and $\boldsymbol{k}_0$ and $\boldsymbol{k}_1$ are the wave vectors of the incoming and outgoing trajectories, respectively. $W(\boldsymbol{q})$ is the square of the Fourier transform of the probe-atom interaction:

$$W(\boldsymbol{q}) = \left\{\int \mathrm{e}^{\mathrm{i}\boldsymbol{q}\cdot\boldsymbol{r}}V(\boldsymbol{r})\,\mathrm{d}\boldsymbol{r}\right\}^2, \tag{2}$$

with $\hbar\boldsymbol{q} = \hbar\boldsymbol{k}_0 - \hbar\boldsymbol{k}_1$ the momentum transfer. It is only $W(\boldsymbol{q})$ and m that are different for electrons and neutrons. $W(\boldsymbol{q})$ is a property of the particle-atom interaction, the Coulomb interaction for electrons and the strong interaction for neutrons. On the other hand $S(\boldsymbol{q},\omega)$, the dynamical structure factor, is solely a target property. The factorization of the cross section in a target part ($S(\boldsymbol{q},\omega)$) and an interaction part is a property of the first Born approximation.

For electron scattering this approach has been used extensively to study the dynamical structure factor related to *electronic* density fluctuations [21,22]. These experiments are referred to as electron energy loss spectroscopy (EELS). In practice a great deal of information was obtained for the electronic $S(\boldsymbol{q},\omega)$ from these electron-energy loss experiments. For example, for the free electron metals one determined with great success the plasmon energy and its dispersion. However at large momentum transfer $S(\boldsymbol{q},\omega)$ of the electronic system is so small that its contribution is swamped by multiple scattering (quasi-elastic scattering from the nuclei with momentum transfer close to q in combination with an electronic excitation with energy ω and $\mathbf{q} \simeq 0$). Hence probing of the *electronic* $S(\boldsymbol{q},\omega)$ for large q values is currently the domain of inelastic X-ray scattering using synchrotron radiation (see e.g. [23]).

Within most of the EELS literature it is tacitly assumed that the energy transfer $\hbar\omega$ due to interactions of the fast electrons with the nuclei is too small to be measured, and hence these interactions are referred to as elastic scattering. Using modern

electron detection technology, and operating at high momentum transfer it was shown recently that, at least for the lighter elements, this assumption is not correct [11], and hence electrons can also be used to measure the nuclear dynamic structure factor $S(\boldsymbol{q}, \omega)$, if Eq. (1) is valid, i.e. the process can be described by the first order Born approximation. This question is not as easily justified for strongly interacting particles such as electrons as it is for weakly interacting neutrons. In the high-energy limit the interaction of an electron with a single atom becomes weak and Eq. (1) should become a reasonable description of the experiment. From gas-phase measurements we know that the differential elastic cross section of $\simeq$40 keV electrons from argon is well described by the first Born approximation but the approximation breaks down for higher Z species such as xenon [24,25]. Thus we expect the first Born approximation (and as a consequence the factorization of Eq. (1)) to provide a reasonable description for 25 keV electrons scattering quasi-elastically from light elements, such as carbon, oxygen and hydrogen.

Neutron scattering experiments have been used to study $S(\boldsymbol{q}, \omega)$ of nuclei over the past decades [5]. At large momentum transfer $\hbar\boldsymbol{q}$ the impulse approximation applies (i.e. the final state of the nucleus, with initial momentum $\boldsymbol{p}$ can be approximated by a plane wave with momentum $\boldsymbol{p} + \hbar\boldsymbol{q}$). In that case the interpretation of $S(\boldsymbol{q}, \omega)$ becomes particularly simple and takes the form

$$S(\boldsymbol{q}, \omega) = \int n(\boldsymbol{p}) \delta\left(\hbar\omega - \frac{(\boldsymbol{p} + \hbar\boldsymbol{q})^2}{2M} + \frac{(p)^2}{2M}\right) \mathrm{d}\boldsymbol{p}. \tag{3}$$

The energy loss of the particle (electron, neutron) $\hbar\omega$ is that expected from scattering of a free particle $(\hbar q)^2/2M$ plus a term proportional to the Doppler shift due to the momentum component of the nucleus along the momentum transfer vector $\hbar\boldsymbol{q}$:

$$\hbar\omega = \frac{(\hbar q)^2}{2M} + \frac{\boldsymbol{p} \cdot \hbar\boldsymbol{q}}{M}. \tag{4}$$

In this limit the energy transfer is just that of a neutron (or electron) scattering from a (classical) particle moving with momentum $\boldsymbol{p}$. The relation between the energy loss $\hbar\omega$ and the atom momentum $\boldsymbol{p}$ can be written as

$$\boldsymbol{p} \cdot \frac{\boldsymbol{q}}{q} = y_M = \frac{M}{q}\left(\hbar\omega - \frac{(\hbar q)^2}{2M}\right). \tag{5}$$

Thus, provided that the mass of the atom is known, measurement of the energy loss and momentum transfer determines the component of $\boldsymbol{p}$ directed along $\boldsymbol{q}$. The observed intensity $J(y_M)$ is thus proportional to the density of atoms with a momentum component y_M along the q direction. This type of a distribution is generally referred to as a Compton profile [5].

An interesting aspect of this process is the scattering time τ_{sc}. As derived by Sears [26] and Watson [5] τ_{sc} does not depend on the details of the scattering process (e.g. velocity of the incoming particle or the range of the interaction) but only on the transferred momentum and the dynamical structure factor of the target. It can be approximated by $\tau_{sc} = 1/qv_0$ with v_0 the root-mean mean velocity of the nucleus before the collision [26]. τ_{sc} is of the order of 10^{-15}–10^{-16} s for scattering from H. Especially at large momentum transfer the collision time is extremely short. The atom does not move significantly during this short time, and hence does not 'feel' the potential due to the surrounding atoms. The target atom acts as a free atom and this is why the impulse approximation applies. The collision resembles that of a collision between two free, classical particles.

The (real) dynamical structure factor $S(\boldsymbol{q}, \omega)$ is the Fourier transform of the (possibly complex) pair distribution function in space and time $G(\boldsymbol{r}, t)$. For classical particles $G(\boldsymbol{r}, t)$ is real, but as Van Hove pointed out [20] at a small enough time scale the quantum nature of any system is expected to reveal itself in a significant imaginary part of $G(\boldsymbol{r}, t)$. Thus at a certain momentum transfer (presently of unspecified magnitude) the quantum nature of $G(\boldsymbol{r}, t)$ is expected to cause deviations from the classical picture sketched before. The anomalous hydrogen cross section at high momentum transfer could be seen as a fingerprint of the complex nature of $G(\boldsymbol{r}, t)$ of protons for small t, as predicted by Van Hove about 50 years ago.

3. Experimental procedure

In this paper we use two specialized techniques that are usually not considered to provide similar information. Here we want to describe the experimental realization of each technique in some detail, emphasizing those aspects that are important for comparing the results.

3.1. Neutron scattering

Experimental details of neutron Compton scattering were described extensively by Karlsson et al. [8]. Here we give a brief description of the experiment to keep the paper self-contained. For the impulse approximation to be valid the scattered neutrons should have an energy of several tens of eV's. Moreover, as we will see, the energy of the neutrons is most conveniently obtained using time-of-flight techniques. Thus one requires a pulsed source of epithermal neutrons. Today these requirements can only be met by a spallation source. Here a pulsed proton beam hits a target and the resulting nuclear reactions produce a flux of very energetic neutrons. After leaving a moderator the neutrons have a whole range of energies from less than an eV up to several hundreds of an eV. A method for spectroscopy using neutrons with energies of several eVs was developed by Brugger et al. [27]. This method is implemented at the Vesuvio (formerly eVs) spectrometer at ISIS where these experiments were done. It uses a combination of time-of-flight and selective absorption techniques and is depicted schematically in Fig. 1. Time-of-flight neutron spectra are taken with and without an absorber between the sample and the detector. In our case an Au absorber was used. It has a narrow absorption line at 4909 meV. The difference of the time-of-flight spectra with and without absorber corresponds thus to neutrons entering the detector with an energy near 4909 meV. These neutrons have all identical (known) flight times from the sample to the detector. Thus the measured time of flight distribution can be directly related to the velocity of the neutrons *before* the interaction with the sample. Typical spectra are shown in Fig. 2. At large scattering angles we see two well-separated peaks. One, at a short time-of-flight, is related to neutrons scattering from protons, the other, at a longer time-of-flight, is from neutrons scattered from the heavier elements (C and O in the formvar case, C only for polyethylene). As the path length of the incoming and outgoing neutrons are known one can convert the time scale in an energy scale of the incoming neutron. This is done in the right panel in Fig. 2. The proton-derived peak is at smaller time-of-flight values and is much broader than the carbon and oxygen related peak. The carbon and oxygen peaks are not separated for detectors at forward angles.

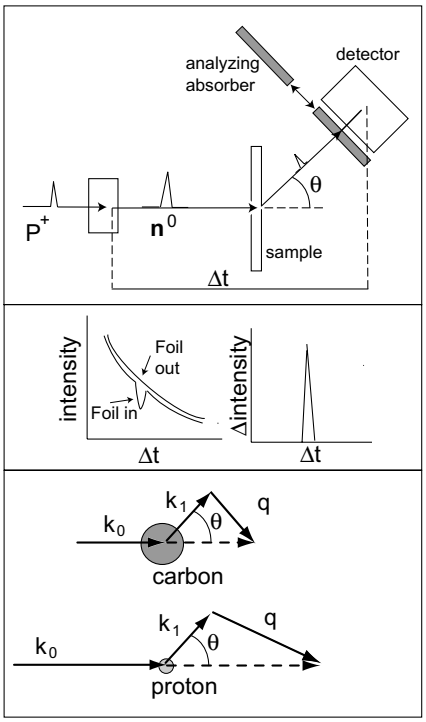

Fig. 1. Schematic view of the Vesuvio spectrometer. In the top panel we sketch the layout. A pulsed proton beam generates a pulsed neutron beam with a wide range of energies. The neutron beam scatters from the sample, and time of flight spectra are recorded with and without the Au absorber in place. The difference of these two spectra (central panel) corresponds to neutrons with a final kinetic energy of 4909 meV and from their time-of-flight Δt one can derive the neutron energy before its interaction with the sample. In the bottom panel we show that the mean momentum transfer measured in a detector is different in size and orientation, for neutrons scattered from H or C.

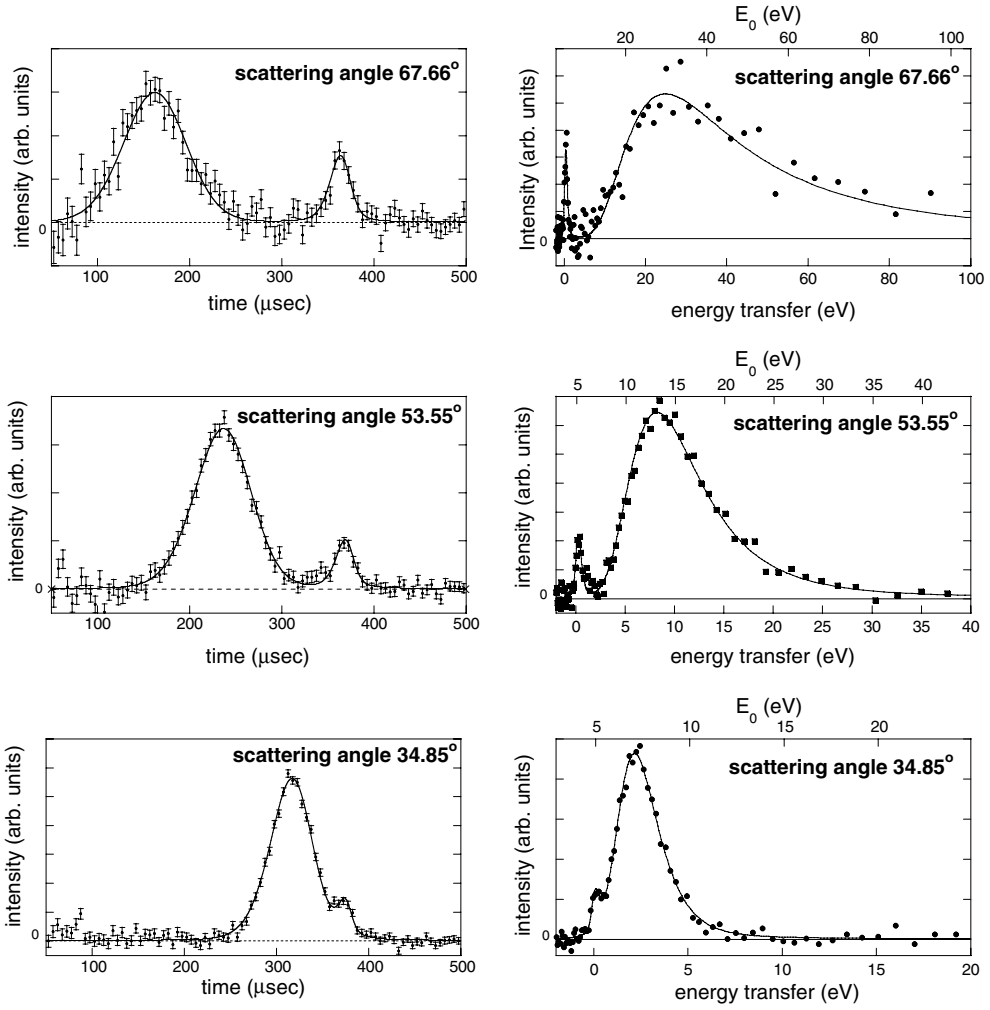

Fig. 2. Neutron time of flight spectra obtained from formvar for different detectors, at scattering angles as indicated, and their corresponding energy transfer spectra. Neutrons scattered from protons cause a peak at smaller time-of-flight values (and hence larger energy transfer values) than those scattered from heavier elements. The solid line is the fit of the time-of-flight spectra assuming two Gaussians in momentum space, one corresponding to neutrons scattered from protons and one to neutrons scattered either from C or O. This fit has been transformed to an energy-scale and plotted as a function of incoming neutron energy E_0 (top axis), as well as the energy transfer (lower axis).

The neutron-nucleus scattering is due to the strong interaction which is of extremely short range. Therefore it can be described by a delta function. One defines the neutron-nucleus potential of a nucleus at $\boldsymbol{r} = 0$ as

$$V(\boldsymbol{r}) = \frac{2\pi\hbar^2}{m_n} b\delta(\boldsymbol{r}), \tag{6}$$

with m_n the mass of the neutron and b is called the scattering length [28,29]. The Fourier transform $V(\boldsymbol{q})$ of $V(\boldsymbol{r})$ is simply $(2\pi\hbar^2/m_n)b$. Thus $V(\boldsymbol{q})$ is isotropic (in the center of mass system) and independent of the magnitude of $\boldsymbol{q}$.

If we substitute this definition of the potential (Eq. (6) into Eq. (1)) and assume that the nucleus is bound (e.g. one describes diffraction in which the nucleus is part of a crystal) which means that $|k_1| = |k_0|$, then one obtains the (bound) cross section by integration: $\sigma_{\text{bound}} = 4\pi|\overline{b^2}|$ i.e. the cross section is that of a 'hard sphere' with radius b. This

cross section for neutron scattering (and hence $|b|$) from different nuclei is accurately known [28].

From Fig. 2 it is clear that the incoming energy E_0 is significantly different for neutrons scattered from C and O compared to those scattered from protons. Even among neutrons scattered from protons there is a large variation in E_0, especially at large scattering angles. Thus the size of the momentum transfer $\hbar\boldsymbol{q}$ (and its direction, see Fig. 1, lower panel) is different for different events contributing to the same time-of flight spectrum. This means also that the phase space factor in Eq. (1) k_1/k_0 varies. It is substantially smaller than 1 for protons, whereas for carbon and oxygen it is much closer to 1.

For formvar it is thus not possible to get directly the ratio of H to (C + O) nuclei using only the cross section and the peak area. Instead the data are fitted by assuming a Gaussian momentum distribution for both constituents (H and C + O). Each Gaussian can be described by two unknowns, its area A_x (proportional to $N_x\sigma_x$, the density of atoms present in the target times the (bound) cross section) and its width (proportional to the vibrational amplitude). From this Gaussian distribution the dynamical structure factor is derived according to Eq. (3), and the experimental data are fitted using Eq. (1). This procedure is described in some detail by Mayers et al. [16] and Karlsson et al. [8]. In this way one can obtain $R_{\mathrm{exp}} = A_{\mathrm{H}}/(A_{\mathrm{C}} + A_{\mathrm{O}})$, the experimentally determined ratio of both contributions. Using conventional theory one would expect this to be equal to $R_{\mathrm{conv}} = N_{\mathrm{H}}\sigma_{\mathrm{H}}/(N_{\mathrm{O}}\sigma_{\mathrm{O}} + N_{\mathrm{C}}\sigma_{\mathrm{C}})$. For polyethylene, a polymer with basic building block CH_2, this simplifies as $N_{\mathrm{O}} = 0$.

The assumption of a Gaussian profile can be justified for isotropic systems bound by harmonic forces. However, in the case of formvar, the use of a single Gaussian for the C + O peak is an approximation only. The concentration of C relative to O was fixed at the nominal ratio for these elements in formvar and the scattering density $N_{\mathrm{C}}\sigma_{\mathrm{C}} + N_{\mathrm{O}}\sigma_{\mathrm{O}}$ is thus known. Now we obtain a fit of the spectrum using these two Gaussians and Eq. (1) as described by Mayers et al. [16,30]. Hence the ratio of the two Gaussians in the fit can be compared with the expected ratio, based on the composition of formvar. This will be done in Section 5.

Recently Cowley has questioned the validity of the experimental procedure followed at Vesuvio [15]. The points raised have been addressed in a recent paper by Mayers and Abdul-Redah [16], a discussion that will not be repeated here.

3.2. Electron scattering

The electron scattering experiment were performed using the $(e, 2e)$ spectrometer of the Australian National University. It was specifically designed for so-called $(e, 2e)$ experiments, and its use for that application is described extensively elsewhere [31]. Here we present some details relevant for the quasi-elastic scattering measurements. Due to the large mismatch in mass of electrons and nuclei, only a small energy transfer occurs, and the Doppler broadening is again less than the mean energy transfer (see Eq. (4)). In order to do these experiments one has to analyze the energy of the scattered electrons (15–30 keV) with a high precision (0.4 eV). At the same time the opening angle of the electron analyzer has to be large enough that the measurement is feasible in a reasonable time (and with a small electron irradiation dose), in spite of the small cross section. Thus the design of the electron optics is crucial for the success of the electron experiment and hence we describe it in some detail.

In contrast to the neutron scattering experiment one uses mono-energetic electrons as an incoming beam. The electrons are emitted by a barium oxide cathode at a potential of $V_{\mathrm{gun}} = -500$ V. The sample is at a positive high voltage (V_{s} between 14.5 kV and 29.5 kV) and hence the impinging electrons have an energy E_0 varying from 15 to 30 keV. After acceleration by V_{s} the incoming beam is collimated by two apertures (0.4 mm and 0.1 mm, respectively, 200 mm apart). The momentum of the incoming electrons is thus known with a high precision ($|\Delta\boldsymbol{k}_0| \simeq 0.1$ Å^{-1}). The electrons impinge on a thin target whose thickness is less than the elastic and inelastic mean free path of the electrons. An electrostatic lens system is placed at 44.3°, followed by a hemispherical energy analyzer. A 0.2 mm wide slit, placed 130 mm away from the sample selects which of the scattered electrons enter the lens system (see Fig. 3). The slit is

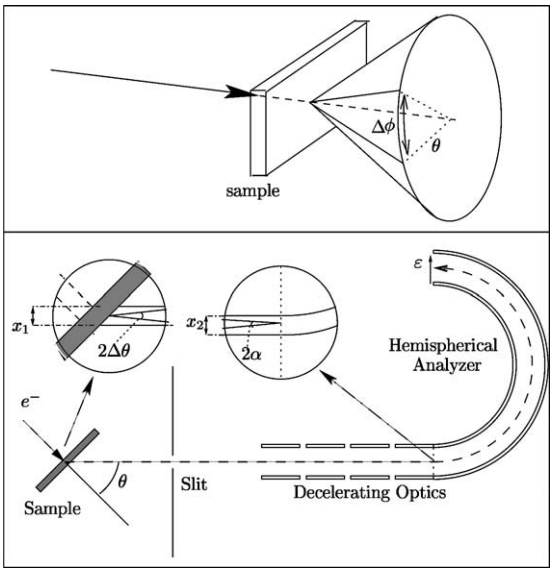

Fig. 3. Outline of the electron scattering experiment. The detector measures electrons scattered over 44.3° within an azimuthal range of $\Delta\phi = 13°$ (top panel). The electron beam hits the sample (spot size x_1) (bottom panel) and enters the decelerating optics with an angular spread $\Delta\theta$. The decelerating optics images the beam spot on the sample at the entrance aperture of the hemispherical analyzer. The optics is adjusted in such a way that the width at the entrance of the analyzer x_2 and angular spread α are optimized for energy resolution, as discussed in the text. The position of the electron at the exit plane of the analyzer depends on its energy ϵ.

not straight, but has the shape of a section of a cone. All electrons transmitted through the slit have been scattered over the same mean θ angle but can have a range of ϕ values. Thus the electrons entering the lens have all been scattered over an accurately known angle θ ($\Delta\theta \simeq 1.7$ mrad). The lens system has the same shape as the slit and is designed to decelerate the electrons (to the pass energy E_{pass} of 400 eV of the hemispherical energy analyzers) and focus these electrons to a (conical) line at the entrance of the analyzer. For a given electron energy the hemispherical analyzer projects an image of the entrance distribution at the exit plane with unit magnification. Electrons with a larger energy will produce an image at the exit plane further out from the center. A detection system formed by a channel plates/resistive anode combination is placed at the exit plane of the analyzer. From the amount of the charge collected at each of the four corners of the resistive anodes one calculates the position at which the incoming electron hits the channel plate, which corresponds in an unique way to the energy of this electron (and to the ϕ angle of the scattering experiment, but this information is not used here). Thus electrons can be measured simultaneously over an energy window of 80 eV and a ϕ range of 10°. The large part of phase space that is measured simultaneously by the analyzer makes the measurement feasible in a relatively short time. Good quality spectra are obtained in half an hour, using a 2–5 nA e^- current.

The lens system (a set of conical slit lenses) focuses only in the θ direction as the ϕ component of the field is always zero. Thus the incoming electrons are focussed along a narrow line forming a section of a cone at the entrance of the hemisphere. Lens settings are chosen in such a way that the width x_2 of this cone segment is of the order of 0.05 mm, half as wide as the spot of the impinging electrons at the sample (0.1 mm) (linear magnification $\simeq$0.5). Following the Helmholtz–Lagrange law ($\Delta x_1 \Delta\theta \sqrt{E_1} = \Delta x_2 \Delta\alpha \sqrt{E_2}$ with Δx_1 the spot size on the target, Δx_2, the width of the image at the entrance of the hemisphere, $\Delta\theta$ the spread in angles accepted by the lens, α the angular spread of trajectories entering the hemisphere, and E_1 and E_2 the energy at the target and in the hemisphere, respectively, see Fig. 3) one expects for this magnification that the angular spread will increase by a factor of $2 * \sqrt{75}$, after deceleration of the beam by a factor of 75 (in the case 30 keV, the highest energy used here). Thus the maximum angular spread α at the entrance of the hemispherical analyzer is 30 mrad.

The dispersive energy analyzer is an electrostatic hemispherical analyzer with mean radius R_0 of 100 mm. The energy resolution is determined by the width of the image x_2 and the aberration of the analyzer. Aberrations of this optical system are proportional to α^2. Hence the energy resolution is given by (see e.g. [32])

$$\frac{\Delta E}{E_{\text{pass}}} = \frac{x_2}{2R_0} + 0.5\alpha^2. \tag{7}$$

Thus at 400 eV pass energy the calculated best possible analyzer resolution is $\Delta E_{\text{anal}} = 0.28$ eV. The observed resolution of the electrons scattered from

heavy elements is $\Delta E_{\mathrm{tot}} = \simeq 0.35 - 0.4$ eV. In that case the Doppler broadening is too small to be resolved. The observed resolution is determined by the analyzer performance and the energy spread of the electron gun (i.e. the thermal spread of the electrons emitted by the BaO cathode): $\Delta E^2_{\mathrm{tot}} = \Delta E^2_{\mathrm{anal}} + \Delta E^2_{\mathrm{gun}}$. The cathode is operating with modest total emission ($\simeq$500 nA) at a relatively low temperature 800 °C corresponding to a thermal spread of 0.23 eV [33]. Thus the observed performance is as good as one can expect.

The momentum transfer for 25 keV electrons scattered over 44.3° is 62.2 Å^{-1} (32.9 a.u.). The energy transfer to a (stationary) proton (mass M_{p}) is $(\hbar q)^2/2M_{\mathrm{p}} = 8.0$ eV, the energy transfer to carbon is 12 times less i.e. 0.7 eV, and for oxygen it is 0.5 eV. Thus the energy separation of the protons induced peak and the main quasi-elastic peak is 7.3 eV for polyethylene and $\simeq$7.4 eV formvar. This separation of more than 7 eV is much larger than the experimental resolution. A series of spectra is presented in Fig. 4 for the case of formvar. Indeed

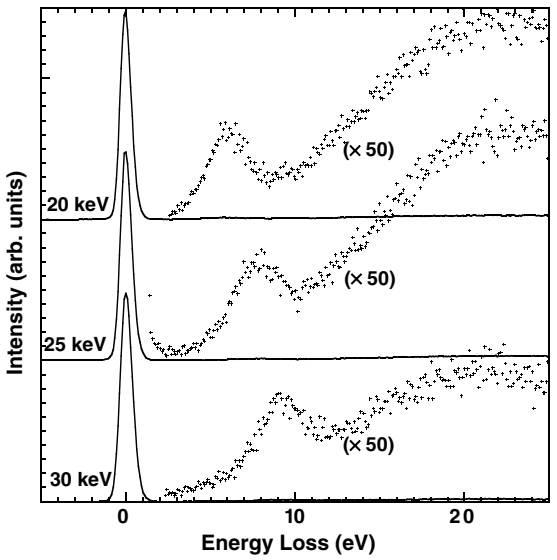

Fig. 4. Some examples of formvar energy loss distributions taken at different electron energies. The large peak near zero energy loss is due to electrons scattered from carbon or oxygen. The small peak moving to larger energy loss values with increasing electron energy is due to electrons scattered from protons.

two peaks are seen with a separation in energy proportional to the incoming beam energy. The peak at larger energy loss values is the proton peak, it is much smaller than the peak associated with electrons scattering from C and O.

The electrons interact with the nucleus by a screened Coulomb interaction. For the light elements present in formvar and polyethylene the screening of the nucleus by its electrons is insignificant for electron scattering at such high momentum transfers as is the case in the present experiment. Thus in good approximation the electron can be considered to scatter from a Coulomb potential of a charge Ze. Thus neglecting the screening one obtains

$$V(q) = \int \frac{Ze^2}{r} e^{i\boldsymbol{q}\cdot\boldsymbol{r}} \mathrm{d}r = \frac{4\pi Ze^2}{q^2}, \tag{8}$$

and using Eqs. (1) and (2) one obtains for the double differential cross section:

$$\frac{\mathrm{d}^2\sigma}{\mathrm{d}\Omega\,\mathrm{d}\varepsilon} = \frac{m^2}{4\pi^2\hbar^5}\frac{k_1}{k_0}\left(\frac{4\pi Ze^2}{q^2}\right)^2 S(\boldsymbol{q},\omega) = \frac{4}{a_0^2\hbar}\frac{k_1}{k_0}\frac{Z^2}{q^4}S(\boldsymbol{q},\omega), \tag{9}$$

with $a_0 = \hbar^2/(me^2)$ the Bohr radius. The scattering cross section is thus proportional to Z^2. Indeed cross section calculations using the partial wave method (taking into account the screening of the nucleus by the electron cloud) reproduce within a percent the same Z^2 dependence of the cross section as Eq. (9) [34]. For scattering from a stationary particle Eq. (9) reduces to the Rutherford double differential cross section.

For the long-range Coulomb force the cross section decreases rapidly with momentum transfer (proportional to $1/q^4$), whereas for the short-range strong interaction, which applies to neutron scattering, it is independent of momentum transfer.

As the energy loss of the 15–30 keV electrons is at most 10 eV, the magnitude of k_1 is smaller than that of k_0 by a negligible amount ($\simeq$0.01 Å^{-1}) and for electron scattering the evaluation of Eq. (1) becomes very straight forward. The peak areas are just proportional to the cross section times concentration.

4. Multiple scattering

Due to the different nature of the electron and neutron probes, multiple scattering has rather different influences on the observed data. In the case of neutrons the particle can enter a detector at an angle θ by a single scattering event over this angle, or by two (or more) scattering events over angle θ_1 and θ_2. The total energy loss due to scattering events over θ_1 and θ_2 is generally not equal to that for scattering over θ. Thus these multiple scattering events will contribute to the spectra at different energies, and will generally cause a broad background in the measured distributions. One can estimate experimentally the importance of multiple scattering by changing the film thickness. Increasing the film thickness will increase roughly linearly the count rate of the single scattering contribution, but the double scattering count rate increase much faster as the probability of scattering over both θ_1 and θ_2 increases [35]. Thus if a significant fraction of the detected particles originate from multiple scattering events the broad multiple scattering background under the Compton peak will increase with target thickness. Experimentally one can conclude that, if the shape of the observed distribution does *not* change after doubling the target film thickness, multiple scattering is not important. Indeed the same shape was found for 0.1 mm and 0.2 mm thick formvar films.

For electrons the same processes hold, but in addition the effects of electronic excitations (referred to as inelastic scattering in the electron literature) have to be considered. The latter ones become important long before multiple deflections from ion cores have a noticeable effect, and we restrict our discussion to that case. In inelastic multiple scattering an electronic excitation occurs, either before or after the deflection from the nucleus. These excitations can range from a single particle excitation (interband transition) to the excitation of a collective mode (plasmon excitation). In either case the associated change in direction is small (of the order of a degree) and the value of θ required for the quasi-elastic scattering event to be detected does not change dramatically. Due to the inelastic scattering these events contribute to the spectra at larger energy loss values. In this way the energy position corresponding to electrons scattered quasi-elastically from carbon (or oxygen) *plus* an appropriate inelastic excitations can be the same as for electrons scattered from a proton. As the cross section for quasi-elastic scattering from carbon and oxygen is much larger than that for quasi-elastic scattering from protons, these inelastic multiple scattering events cause a significant background under the proton-related peak, even for the thinnest films. Again halving the film thickness would cause a corresponding decrease of the multiple scattering contribution relative to the single scattering contribution, but in practise there are limits to how thin one can make a film. Increasing the beam energy, and decreasing the scattering angle in such a way that the transferred momentum is constant is in principle another option, but not feasible with the present spectrometer. Doubling the beam energy would roughly half the inelastic multiple scattering contribution and, for a given momentum transfer $\hbar\boldsymbol{q}$ (i.e. a smaller scattering angle) the differential cross section would stay the same (Eq. (9)).

In summary multiple scattering effects in the neutron experiment refer to multiple deflections of the neurons, whereas multiple scattering effects in the electron experiment refer mainly to inelastic collisions of the probing electron.

5. Comparison of electron and neutron results

For the electron scattering experiments one needs extremely thin self-supporting polymer films ($\simeq$10 nm thick). Moreover the electron energy loss spectrum should not display strong features at similar loss values as the electrons scattered from protons. Many unsaturated polymers have a pronounced peak near 6 eV energy loss due to π–π^* electronic transitions, and are hence less suitable. Thus we have chosen formvar, well- known in electron microscopy research to give thin films with a featureless loss spectrum, and polyethylene, the most simple saturated polymer.

5.1. Formvar

There are two important quantities accessible by both techniques: the width of the proton peak

and the area of the proton peak compared to that of the C + O peak. Let us first compare the shape of the proton peak. This is in itself an important quantity as it reflects the momentum distribution of the protons. Moreover in the case of electron scattering the shape of the distribution could be affected by structures present in the background, that do not resemble the smooth line used for the subtraction. In that case the shape of the proton peak for electrons would be different from that of neutrons.

For both the electron and neutron experiment the measured width of the C + O peak is much smaller than that of the proton peak, setting an upper limit to the contribution of the experimental resolution to the observed width. The experimental contribution to the width of the proton peak is thus negligible.

For neutrons one determines for each time-of-flight data point, the incoming momentum $\hbar\boldsymbol{k}_0$ and uses this to determine the momentum transfer $\hbar\boldsymbol{q}$ for each time-of-flight data point, as $\hbar\boldsymbol{k}_1$ is determined by the absorption energy (4909 meV) of the analyzer foil (see Fig. 1). Then one can simply apply Eq. (5) to determine the momentum component $\boldsymbol{p}$ along the $\boldsymbol{q}$ direction. This direction will change slightly as a function of k_0 but this causes no complication for isotropic materials.

For electrons one first has to subtract the multiple scattering background. This is done by fitting the background by a third order polynomial plus a Gaussian tail from a peak located at the mean energy loss position of carbon and oxygen. For the high-energy data (20 keV, 25 keV, 30 keV) this was relative straight forward. For the 15 keV measurement the peak separation becomes small and the background choice is somewhat arbitrary. We can get some guidance from the fact that the general shape of all 4 spectra *without* the proton peak should be similar. It is basically an energy loss spectrum, with a shape that, for thin films, is independent of the probing energy [22]. Different

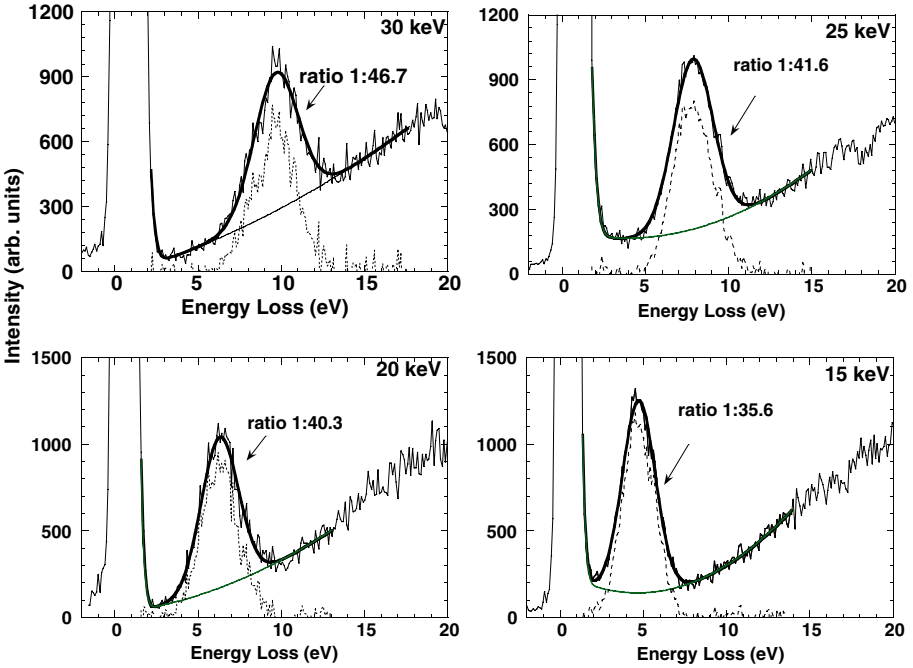

Fig. 5. A fit of the hydrogen part of the formvar electron scattering spectra. All spectra are normalized in such a way that the main (carbon + oxygen related) quasi-elastic peak has 1 000 000 counts. The estimated area of the proton peak is shown as well. Based on the Z^2 dependence of the cross section and the formvar stoichiometry one expects the proton peak area to be 29.7× less than the main peak area. The observed proton peak area is systematically smaller than predicted by the Z^2 dependence.

choices of background can affect the area by ≃10%. The results of these fits are shown as a solid line in Fig. 5.

After background subtraction one can straightforwardly transform the electron energy loss scale to a momentum scale of the proton momentum component y. As $\boldsymbol{q}$ is identical for all energy losses this is simply obtained by applying Eq. (5), i.e. by subtracting the term $(\hbar q)^2/2M$ followed by a multiplication with constant factor $M/(\hbar q)$. The result, a projection of the proton momentum density $J(y)$, was published in [12] and is reproduced in Fig. 6. In this figure we show the results of the 4 electron energies together with the fit of the neutron data for a representative detector. Clearly the agreement is excellent.

In Fig. 7 the measured width of the proton momentum distribution is plotted as a function of the mean momentum transfer. The statistical error in both methods is comparable and no clear dependence of the width on the momentum transfer is found. Both electron and neutron measurements appear to show a minimum in width around 60 Å^{-1}, but we have no physical model that would produce this kind of behavior. The width is a signature of the strength of the chemical bond of the hydrogen atoms with carbon. A strong bond tends to localize the hydrogen wave function in real space, and hence lead to a broad distribution in momentum space.

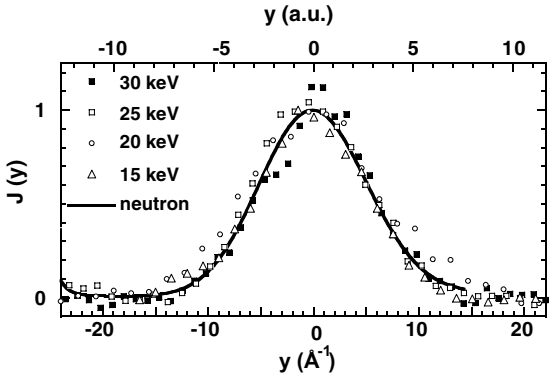

Fig. 6. The Compton profiles of protons in formvar as obtained by electron scattering at different energies, as indicated. A single fit of neutron Compton profiles is shown as well for comparison. All distributions are scaled to equal height.

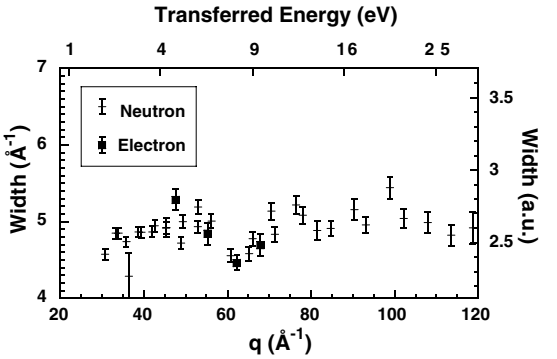

Fig. 7. The width of the Compton profile of protons in formvar as measured using neutrons and using electrons as a function of momentum transfer $\boldsymbol{q}$.

Now we compare the relative area of the hydrogen peak as obtained by neutron scattering and by electron scattering. From the composition of formvar ($C_8O_2H_{14}$) we know that the carbon-to-oxygen ratio is 4:1 and use a weighted cross section for the analysis. Neither technique resolves the carbon contribution from the oxygen one, and hence we have no way of verifying this ratio. Assuming the nominal formvar stoichiometry one can calculate the expected hydrogen peak area relative to the sum of the oxygen and carbon area. The experimentally obtained intensity R_{exp} as a fraction of the ratio predicted by conventional theories (R_{conv}) was obtained in [12] and is plotted again in Fig. 8. The measured hydrogen peak area was considerably smaller than expected. This shortfall in hydrogen peak area has been attributed to quantum entanglement at short time scale of the measurement. This surprising fact has been discussed elsewhere [12]. Notice that with increasing momentum transfer, when shorter scattering times apply, the shortfall of the hydrogen signal increases.

The experimental resolution of the electron experiment is currently determined for a significant part by the thermal energy spread of the electrons emitted by the barium-oxide cathode. It could be replaced by a monochromator, which could easily reduce the energy spread below 100 meV. However even for the C + O peak the Doppler broadening dominates the observed width (experimentally found peak width 0.6 eV, whereas for electrons scattered from heavy nuclei one obtains a width

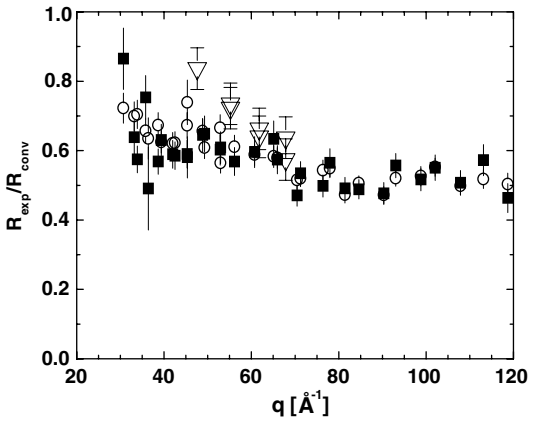

Fig. 8. The measured hydrogen intensity as a function of momentum transfer normalized relative to the expected intensity based on the known cross sections. Two different electron measurements are indicated by triangles (up and down). Full squares (open circles) represent results from neutron measurements of formvar foils of 0.1 mm (0.2 mm) thickness.

of 0.4 eV). Thus for the study of formvar increased energy resolution would be of limited value.

The energy resolution of the neutron experiment is determined by the width of the absorption dip of the gold foil. The shape of the absorption is determined by a combination of a Gaussian (due mainly to thermal motion of the Au atoms (standard deviation 33 meV)) and a Lorentzian distribution (due to the life-time broadening of the Au nuclear excited state (HWHM 143 meV)). The absorption shape is determined from spectra obtained from Pb, where Doppler broadening is very small. The Lorentzian contribution to the line shape causes long-range tails to the Compton profiles. It has been suggested that these long-range tails are the root of the observed anomalies [36,37]. Hence it is important to improve the resolution of the neutron experiment. The number of suitable resonances that can be used as an absorber is limited, and the width of the resonance could be expected to set strict limits to the resolution one can obtain with these foils. However a large part of the Lorentzian tail can be removed by the so-called double difference method [38,39]. In this method three time-of-flight spectra are obtained, one without an absorber, one with an absorber of 0.0125 mm thick, and one with an absorber three times this thickness. Near the resonance energy the thick foil absorbs so strongly, that the transmitted amount is non-linear to the foil thickness. In the wings the absorption is much less, and one is still in the linear regime. Thus by subtracting three times the thin absorption spectrum from the thick absorption spectra one expects the contribution of the wings to cancel, whereas near the resonance there is a remainder of intensity. The resulting spectra can be fitted with a line shape with a much smaller Lorentzian contribution (convolution of a 82 meV (standard deviation) Gaussian plus a 22 meV (HWHM) Lorentzian contribution). The resulting spectra are displayed in Fig. 9. The difference is especially noticeable for the C + O part of the spectrum. However the increase in resolution is offset by a decrease in statistical accuracy. Similar anomalies for hydrogen are obtained using the single and double difference method. The fact that consistent areas are obtained is a strong indication that the anomaly is not an artifact of the way the fitting procedure deals with the Lorentzian tails.

5.2. Polyethylene

Low density polyethylene foil (Goodfellows ET311251, 0.15 mm thick) was used directly for the neutron experiment. For the electron experiment thin samples ($\simeq$10 nm) were obtained using a method derived from the procedure described by Cranfill [40] and the one described by Godovsky and Magonov [41]. The polyethylene was dissolved in xylene at 100 C (0.1% w/w). A microscope slide was partly submerged in the xylene, and after it was thermally equilibrated it was slowly (0.5–1 cm/min) pulled out of the hot solution. After cooling down and drying the microscope slide was slowly submerged in distilled water (with a 10–20° angle between the microscope slide and water surface). The polyethylene film separates from the microscope slide and floats on the water surface. Subsequently it is picked up on the micro-screen (Buckbee Mears, 0.25 mm diameter holes) of the sample holder. Up to a few hundred holes were covered with a thin film. Suitable thin parts were selected by observing the singles count rate in the detector.

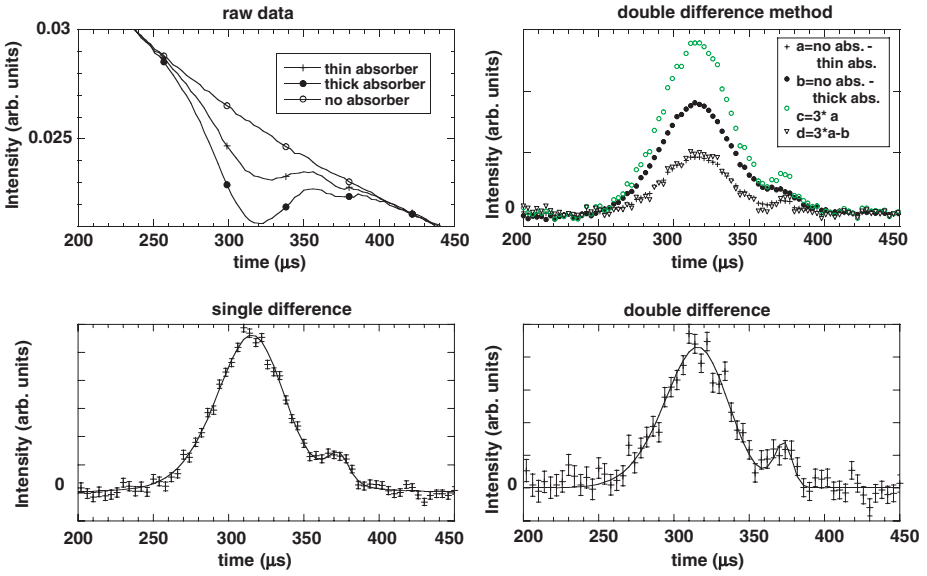

Fig. 9. Neutron time of flight spectra of formvar obtained with the single thickness and triple thickness absorber (top left). The absorption effect in the single difference spectra of the thick absorber (line *b*, top right) is near the peak not three times that of the single difference spectra of the thin absorber (line *a*), but in the tails it is three times stronger. Hence the tails are suppressed in line *d*, obtained from a subtraction of the single difference spectra $d = 3 * a - b$. The suppression of the Lorentzian tails in the double difference method causes a better separation of the carbon/oxygen peak and the proton peak (bottom panels). The fit of the double difference spectra is obtained with a line shape with much reduced Lorentzian character.

The electron scattering spectra and their fits are shown in Fig. 10. For the 15 keV incident energy a peak is seen at 4.4 eV below the main quasi-elastic peak, moving to higher binding energy with increasing incident energy. The loss features are again $\simeq 50\times$ weaker than the main quasi-elastic peak, indicating similar film thickness as the formvar films. The peak stands out somewhat more clearly. This is expected as the hydrogen content in polyethylene is high. Neutron data were taken using a single, 0.15 mm thick polyethylene film. Qualitatively very similar spectra as those for formvar were obtained. The neutron fitting procedure was straightforward, as the heavy element consisted of only one element (carbon). Using the same procedure as for the formvar film we obtain a width of the hydrogen distribution, plotted as a function of momentum transfer in Fig. 11. Very similar widths were observed in an earlier neutron Compton study of polyethylene [42]. Also the width of the hydrogen peak is very similar in polyethylene and formvar, not surprisingly as the bond strength of the carbon–hydrogen bond does not depend strongly on the type of polymer. However the dip observed for formvar near 60 Å^{-1} of transferred momentum is not reproduced for polyethylene, supporting the view that it is only a statistical fluctuation. Again a good agreement was found for both electrons and neutrons.

As the electron scattering cross section (Eq. (9)) is proportional to Z^2 and the hydrogen concentration is twice that of carbon we expect the hydrogen peak area to be 18 times smaller than the carbon peak area. The measured hydrogen to carbon ratio is between 1:24 and 1:29 showing again that the hydrogen intensity is significantly less than expected (Fig. 12).

The electron measurement could be affected, in principle, by the very small structures known to exist in the inelastic energy loss spectra of polyethylene, in the 7–10 eV range (see [43]), or due to possible residual xylene that is expected to have a peak near 7 eV [44]. These features all would contribute by multiple scattering (deflection from the carbon nucleus plus inelastic event with an energy loss value in the 7–10 eV range) in the same region

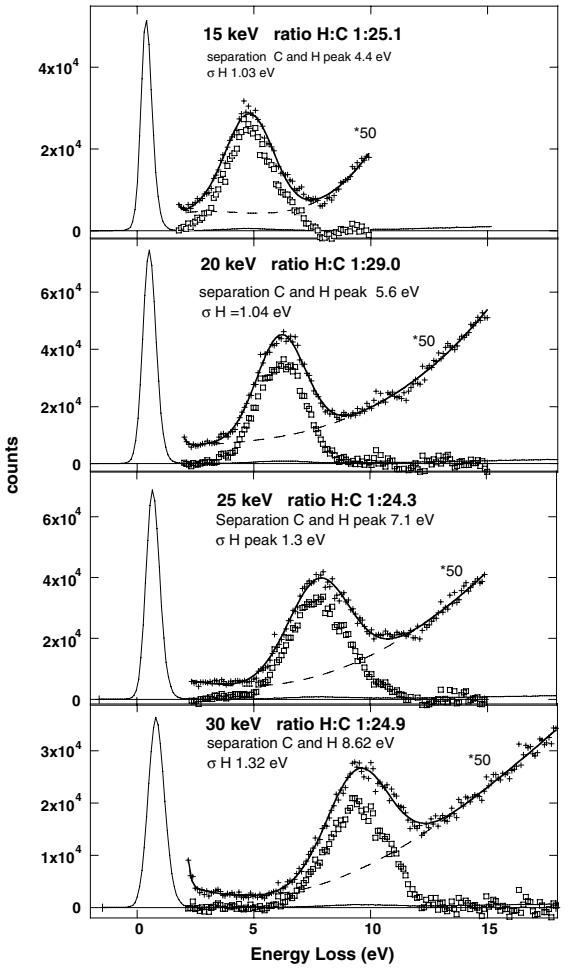

Fig. 10. The electron spectra of a polyethylene film for electron energies as indicated. The hydrogen part is magnified 50 times and fitted as described in the text (full line). The decomposition of the hydrogen peak (dots) into background (dashed) and signal (circles) is displayed as well.

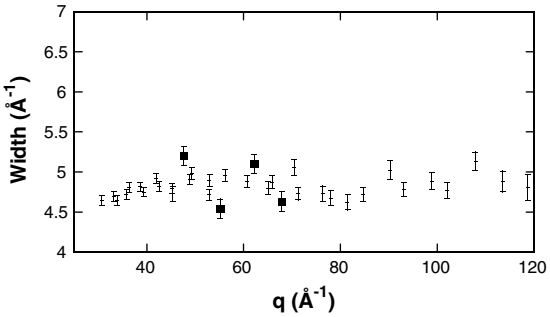

Fig. 11. The width of the Compton profile of protons in polyethylene as measured using neutrons and using electrons as a function of momentum transfer.

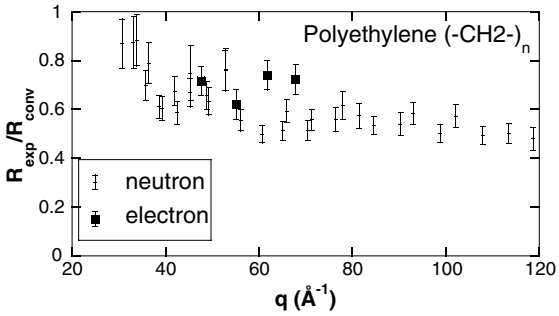

Fig. 12. The measured hydrogen peak area compared to the expected peak area for the polyethylene film for both electrons and neutrons.

as where the proton peak appears, and this would lead generally to a larger areas of the proton peak, rather than the smaller areas observed. Contributions of this type, if present in a significant level, would affect the peak position, width and area differently for different incoming energies, as the proton peak moves with this energy. The facts that peak width consistent with the neutron measurements are obtained and good agreement is found for the expected and measured proton peak positions show that these energy loss features contribute at most in a very minor way. Also the fact that consistent results are obtained between formvar and polyethylene makes it extremely unlikely that the large anomalies observed are due to structures in the background.

6. Radiation damage

The probing beam could affect the sample composition and this should be cause of the anomalous hydrogen concentration. For the neutron experiments this effect is known to be completely negligible. For electrons one should be more careful, as not just the recoil but also electronic excitations may cause sample decomposition and associated hydrogen release. Unfortunately there are very limited experimental data, as hydrogen is not easily detected directly. Therefore we studied the

change in polyethylene sample composition as a function of total accumulated dose during the measurement. Instead of accumulating for half an hour we accumulated for 2 min intervals using a small beam current of 1.6 nA. In spite of the limited statistics reasonable fits could be obtained for the two minute spectra. Peak position and width (σ) were free fitting parameters, but the difference between the maximum and minimum values found was only 0.12 eV and 0.17 eV, respectively, indicating that the statistics was good enough to obtain meaningful fits. The results are shown in Fig. 13. There is a small tendency of the hydrogen:carbon ratio to decrease with time, but these changes are an order of magnitude smaller than the anomalies observed.

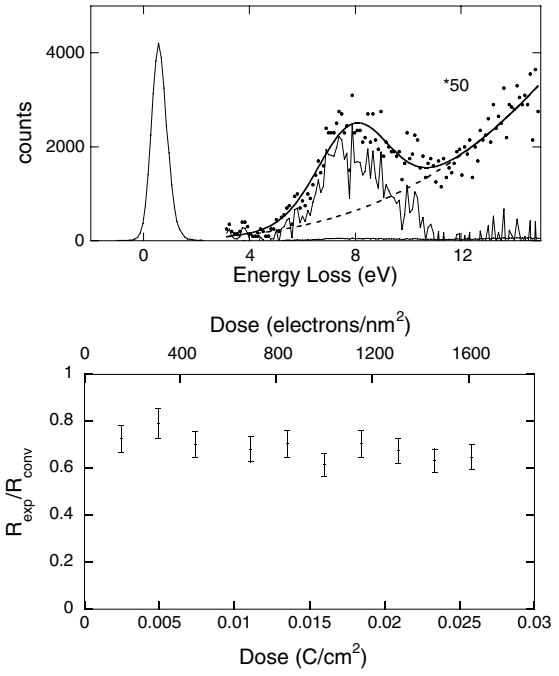

Fig. 13. The top panel shows the quality of a polyethylene spectrum obtained in two minutes and the decomposition of the signal (dots) in background (dotted line) and proton signal (full line, magnified part). A series of 2 minute measurements was performed. The dependence of the R_{exp}/R_{conv} (measured hydrogen peak area relative to the expected peak area) as a function of accumulated beam charge is displayed in the lower panel. The R_{exp}/R_{conv} ratio decreases slowly with dose. However this decrease is much too slow to explain the observed anomaly.

Radiation damage in polyethylene has been studies by observing the disappearance of diffraction spots in polyethylene crystals by Grubb and Groves [45]. They observed (for a beam energy of 100 keV) the disappearance of the long range order at doses near 0.01 C/cm^2. However the relation between hydrogen loss and the disappearance of long-range order is not straight forward. Similar conclusions apply to formvar [46]. Thus in our experiment the ratio of the main quasi-elastic peak to the hydrogen peak is only a mild function of accumulated electron dose.

7. Conclusion

We compared electron and neutron scattering measurements of the double differential cross section of protons in two polymers. The theoretical framework described in Section 2 predicts that both methods should reveal the same information about the motion and concentration of protons. Indeed electron and neutron results are consistent. The same momentum distribution was found and this distribution is in line with the calculated carbon–hydrogen bond strength. For both electron and neutron experiment the measured hydrogen concentration deviates strongly (15–40%) from what is derived from well known cross sections. Similar values were found for polyethylene and formvar, in spite of the different sample preparation procedures of the thin films for the electron scattering experiment. These results are consistent with the interpretation that protons can not be considered as classical particles but are quantum-entangled with adjacent electrons at the short time scale of the electron/neutron–proton collision [19].

The main advantage of the neutron experiment is that it can measure thick (bulk) samples and samples with relatively low hydrogen contents. The electron experiment requires extremely thin samples with very large hydrogen concentration. Its data-analysis is somewhat more direct, and the infra-structure required is more modest. The electron scattering experiment could be developed in a form that allows for the measurement of gas-phase species, and could possibly form the basis

for a technique that detects hydrogen in an electron microscope.

Recently it was suggested that the coherence length of the probing particle is an important parameter in interpreting these data [47]. The coherence length $l_{coh} = \lambda^2/2\Delta\lambda$ of the electron and neutron probe are completely different. For neutrons it is determined by the width in energy of the absorption used and it corresponds to approximately 2.5 Å. For electrons it is determined by the thermal spread of the electrons emitted by the gun and for 25 keV electrons with an energy spread of 0.4 eV the coherence length is of the order of 400 Å. Thus in all cases the mean H–H distance is smaller than the coherence length of the applied probe.

The neutron and electron results are obtained by completely different experimental techniques and data analysis procedures. Therefore the fact that both neutrons and electrons measure 'anomalous' hydrogen concentration indicates that it is not due to an experimental artifact, but is a genuine effect of the condensed matter systems under investigation here.

Very recently it was shown at McMaster University (Canada) that the carbon and proton signal can be separated as well for elastic scattering of electrons from methane in the gas phase [48]. Also researchers at Atomki (Hungary) have shown recently that the same is true for an electron scattering experiment in which electrons are backscattered from a thick polymer film [49]. Thus electron scattering experiments are possible under a wider range of conditions, than those described in this paper. Detailed analysis of these measurements should help elucidating the 'anomalous' scattering results.

Acknowledgements

M.V. wants to thank B. McEachran for helpful discussion, and financial support of the AMRFP program. This work was partially supported by the Australian–German (DAAD) Joint Research Co-operation Scheme. C.A.C.-D. acknowledges helpful discussions with E.B. Karlsson and support, in parts, by the Fonds der Chemischen Industrie, the EU network QUACS, and a grant from the Royal Swedish Academy of Sciences.

References

[1] H. Boersch, R. Wolter, H. Schoenebeck, Z. Phys. 199 (1967) 124.
[2] D. Varga, K. Tökesi, Z. Berènyi, J. Tóth, L. Körvér, G. Gergeley, A. Sulyok, Surf. Interface Anal. 31 (2001) 1019.
[3] P.C. Hohenberg, P.M. Platzman, Phys. Rev. 152 (1966) 198.
[4] H. Rauh, N. Watanabe, Phys. Lett. A 100 (1984) 244.
[5] G.I. Watson, J. Phys.: Condens. Matter 8 (1996) 5955.
[6] C.A. Chatzidimitriou-Dreismann, T. Abdul-Redah, R.M.F. Streffer, J. Mayers, Phys. Rev. Lett. 79 (1997) 2839.
[7] T. Abdul-Redah, R.M.F. Streffer, C.A. Chatzidimitriou-Dreismann, B. Hjörvarsson, E.B. Karlsson, J. Mayers, Physica B 276–278 (2000) 824.
[8] E.B. Karlsson, T. Abdul-Redah, R.M.F. Streffer, B. Hjörvarsson, J. Mayers, C.A. Chatzidimitriou-Dreismann, Phys. Rev. B 67 (2003) 184108.
[9] C.A. Chatzidimitriou-Dreismann, T. Abdul-Redah, R.M. Streffer, J. Chem. Phys. 116 (2002) 1511.
[10] C.A. Chatzidimitriou-Dreismann, T. Abdul-Redah, B. Kolarić, J. Am. Chem. Soc. 123 (2001) 11945.
[11] M. Vos, Phys. Rev. A 65 (2002) 12703.
[12] C.A. Chatzidimitriou-Dreismann, M. Vos, C. Kleiner, T. Abdul-Redah, Phys. Rev. Lett. 91 (2003) 57403.
[13] A. Ioffe, M. Arif, D.L. Jacobson, F. Mezei, Phys. Rev. Lett 82 (1999) 2839.
[14] C.A. Chatzidimitriou-Dreismann, T.A. Redah, R.M.F. Streffer, B. Hessmo, Phys. Rev. Lett. 84 (2000) 2036.
[15] R.A. Cowley, J. Phys: Condens. Matter 15 (2003) 4143.
[16] J. Mayers, T. Abdul-Redah, J. Phys.: Condens. Matter 16 (2004) 4811.
[17] E. Karlsson, S. Lovesey, J. Phys.: Condens. Matter 16 (2004) 5631.
[18] D. Colognesi, Physica B 344 (2004) 73.
[19] C.A. Chatzidimitriou-Dreismann, J. Alloys Comp. 356–357 (2003) 244.
[20] L. Van Hove, Phys. Rev. 95 (1954) 249.
[21] P.M. Platzman, P.A. Wolff, in: F.S.H. Ehrenreich, D. Turnbull (Eds.), Solid State Physics, Vol. 13, Academic Press, New York, 1973, p. 1.
[22] J. Fink, M. Knupfer, S. Atzkern, M.S. Golden, J. Electron. Spectrosc. Relat. Phenom. 117–118 (2001) 287.
[23] W. Schülke, J. Phys.: Condens. Matter 13 (2001) 7557.
[24] M. Fink, J. Kessler, Z. Phys. 196 (1966) 1.
[25] M. Fink, R.A. Bonham, Phys. Rev. 187 (1969) 114.
[26] V.F. Sears, Phys. Rev. B 30 (1984) 44.
[27] R.M. Brugger, A.D. Taylor, C.E. Olsen, J.A. Goldstone, A.K. Soper, Nucl. Instr. and Meth. 221 (1984) 393.

[28] S. Lovesey, Theory of Neutron Scattering from Condensed Matter, Vol. 1, Clarendon Press, Oxford, 1984.
[29] G. Squires, Introduction to the Theory of Thermal Neutron Scattering, Cambridge University Press, Cambridge, 1978.
[30] J. Mayers, T.M. Burke, R.J. Newport, J. Phys.: Condens. Matter 6 (1994) 641.
[31] M. Vos, G.P. Cornish, E. Weigold, Rev. Sci. Instr. 71 (2000) 3831.
[32] J.H. Moore, C.C. Davies, M.A. Coplan, Building Scientific Apparatus, Addison-Wesley, London, 1983.
[33] W. Franzen, J.H. Porter, Adv. Electron. Electron. Phys. 39 (1975) 73.
[34] F. Salvat, R. Mayol, Comp. Phys. Commun. 74 (1993) 358.
[35] J. Mayers, A.L. Fielding, R. Senesi, Nucl. Instr. and Meth. A 481 (2002) 454.
[36] J.J. Blostein, J. Dawidowski, J.R. Granada, Physica B 304 (2001) 357.
[37] J. Blostein, J. Dawidowski, J. Granada, Physica B 334 (2003) 257.
[38] R.J. Newport, J. Penfold, W.G. Williams, Nucl. Instr. and Meth. 224 (1984) 120.
[39] P.A. Seeger, A.D. Taylor, R.M. Brugger, Nucl. Instr. and Meth. A 240 (1985) 98.
[40] B. Cranfill, Rev. Sci. Instr. 49 (1978) 264.
[41] Y.K. Godovsky, S.N. Magonov, Langmuir 16 (2000) 3549.
[42] B. Gabrys, W. Zajac, J. Mayers, M. Kalhoro, Appl. Phys. A 74 (Suppl.) (2002) S1645.
[43] M. Barbarez, D.D. Gupta, D. Hayward, J. Phys. D 10 (1977) 1789.
[44] U. Killat, J. Phys. C 7 (1974) 2396.
[45] D. Grubb, G. Groves, Philos. Mag. 24 (1971) 815.
[46] M. Vos, Ultramicroscopy 92 (2002) 143.
[47] E.B. Karlsson, Phys. Rev. Lett. 90 (2003) 95301.
[48] G. Cooper, A.P. Hitchcock, unpublished.
[49] D. Varga, Z. Berényi, K. Tökési, J. Tóth, L. Kövér, I. Cserny, unpublished.